Printed ISSN 1330–0016
Online ISSN 1333–9133
CD ISSN 1333–8390
CODEN FIZBE7

TAGGING EMC EFFECTS AND HADRONIZATION MECHANISMS BY SEMI-INCLUSIVE DEEP INELASTIC SCATTERING OFF NUCLEI

CLAUDIO CIOFI DEGLI ATTI[a], LEONID P. KAPTARI [a,b] and CHIARA BENEDETTA MEZZETTI[a]

[a]*Department of Physics, University of Perugia and INFN, Sezione di Perugia, Via A. Pascoli, I-06123, Italy*

[b]*On leave from Bogoliubov Lab. Theor. Phys., JINR, Dubna, 141980, Russia*

Received 31 January 2011; Accepted 16 November 2011
Online 26 January 2012

The semi-inclusive deep inelastic scattering of electrons off a nucleus A with detection of a slow nucleus $(A-1)$ in the ground or low excitation states, i.e. the process $A(e,e'(A-1))X$, can provide useful information on the origin of the EMC effect and the mechanisms of hadronization. The theoretical description of the process is reviewed and the results of several calculations on few-body systems and complex nuclei are presented.

PACS numbers: 13.40.-f, 21.60.-n, 24.85.+p,25.60.Gc UDC 539.126
Keywords: SIDIS, EMC effect, final state interaction, hadronization, few nucleon systems

1. Introduction

In spite of many experimental and theoretical efforts (for a recent review see Ref. [1]), the origin of the nuclear EMC (European muon collaboration) effect has not yet been fully clarified and the problem as to whether and to what extent the quark distribution of nucleons undergoes deformations due to the nuclear medium remains open. At the same time, information on in-medium hadronization, to date, comes mainly from the measurement of the multiplicity ratio of the lepto-produced hadrons in semi-inclusive deep-inelastic scattering (SIDIS) off nuclei $A(e,e'h)X$ depicted in Fig. 1 (left) (for a recent review see Ref. [2]). This type of SIDIS, investigated by the HERMES experiment at HERA, as well as at JLab [2], has provided relevant information on different models of hadronization in the medium [3 – 6]. However, some important details of the hadronization mechanism are still missing, in particular, it is difficult by the SIDIS process $A(e,e'h)X$ to obtain information on the early stage of hadronization; for such a reason, other types of SIDIS processes should be investigated in order to improve our knowledge on hadronization in the medium. To this end, the process $A(e,e'(A-1))X$, depicted in one photon approximation in

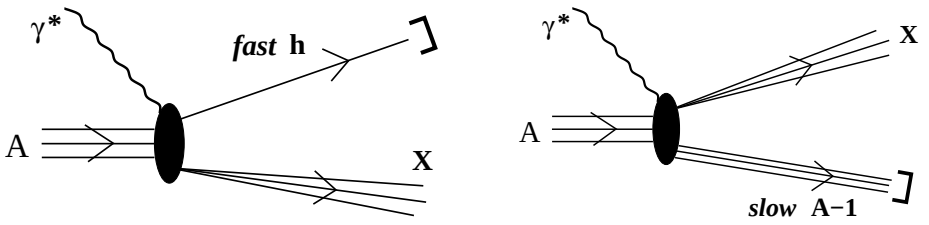

Fig. 1. Left: The "classical" SIDIS process $A(e,e'h)X$ in one-photon exchange approximation: the fast hadron h, that originated from the leading quark hadronization, is detected in coincidence with the scattered electron e'. Right: the new SIDIS processes $A(e,e'(A-1))X$; here a nucleus $(A-1)$ is detected in coincidence with the scattered electron e'.

Fig. 1 (right), has been proposed in Ref. [7] within the so called spectator mechanism, according to which the virtual photon γ^* interacts with a quark of a nucleon of the target A and the "spectator" nucleus $(A-1)$ recoils by momentum conservation and is detected in coincidence with the scattered electron. In Ref. [7], however, the plane wave impulse approximation (PWIA) (diagram Fig. 2(a)) has been used, so that some of the results were only of qualitative character. An important step forward in the investigation of the new SIDIS process was made in Ref. [8], where the theoretical approach has been extended by considering the final state interaction (FSI) of the hadronizing debris (the leading quark and the diquark) with the nucleons of the nucleus $(A-1)$ (diagram 2(b)) in terms of an effective debris-nucleon interaction cross sections derived on the basis of the hadronization model of Ref. [3]. Once the propagation and interaction of the debris with the spectators are taken into account, the advantages of the SIDIS process $A(e,e'(A-1))X$ become clear. Concerning the hadronization mechanism, it has been shown [8] that the survival probability of the recoil nucleus $(A-1)$ is very sensitive to the details of the rescattering and hadronization of the debris, i.e. to the mechanism of the hadronization. Moreover, a clear advantage of the process under discussion, compared to leading hadron production, is the possibility to study the early stage of hadronization at

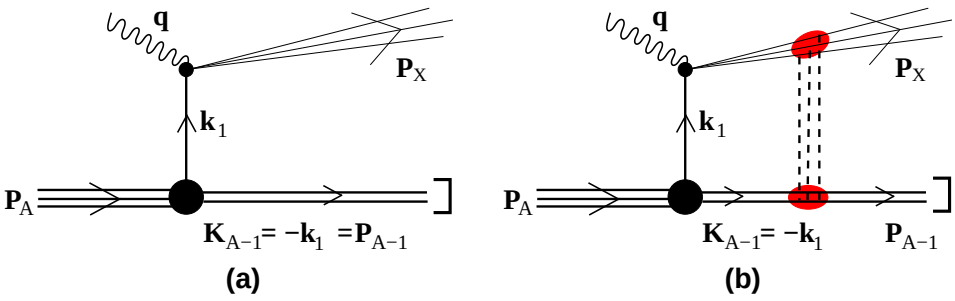

Fig. 2. The Feynman diagrams corresponding to the PWIA (a) and the FSI (b) cross sections of the SIDIS process $A(e,e'(A-1))X$ within the spectator mechanism.

short formation times without being affected by cascading processes. Indeed, no cascading is possible if the recoiling nucleus $(A-1)$ survives. At the same time, most of hadrons with small momentum produced in inclusive process $A(e,e'h)X$ originate from cascading of more energetic particles, so that, in order to analyze data and extract information on the early stage of hadronization, a realistic model for cascading is necessary, which is barely possible [8]. As for the investigation of the EMC effects, it has been shown [7] that a properly defined ratio of the cross section on nucleus A, taken at a value of the Bjorken scaling variable x_{Bj}, to the cross section on the same nucleus, taken at a different value of x_{Bj}, is essentially identical to the ratio of the nucleon structure functions $F^{(N/A)}(x_{Bj})/F^{(N/A)}(x'_{Bj})$.

The SIDIS process $A(e,e'(A-1))X$ was almost impossible to access experimentally when it was proposed in 1999, but notable progress has been done since then: in a recent experiment at Jefferson Lab [9, 10], the process $^2\mathrm{H}(e,e'p)X$ has been investigated in detail, finding, as will be shown later on, a gratifying agreement with theoretical results [11, 12]; moreover, experimental proposals have been finalized to study the process on complex nuclei, thanks to the development of proper recoil detectors [13].

The aim of this paper is to review the theoretical description of the process $A(e,e'(A-1))X$ and to present the results of several calculations for both few nucleon systems and complex nuclei.

The SIDIS cross section, which includes FSI, has the following form [11, 12, 14]

$$\sigma^{A,\mathrm{FSI}}(x_{Bj},Q^2,|\mathbf{P}_{A-1}|,y_A,z_1^{(A)}) \equiv \sigma^{A,\mathrm{FSI}} = \frac{\mathrm{d}\sigma^{A,\mathrm{FSI}}}{\mathrm{d}x_{Bj}\mathrm{d}Q^2\mathrm{d}\mathbf{P}_{A-1}} =$$

$$= K^A(x_{Bj},Q^2,y_A,z_1^{(A)}) z_1^{(A)} F_2^{N/A}(x_A,Q^2,k_1^2)\, n_0^{A,\mathrm{FSI}}(\mathbf{P}_{A-1}), \qquad (1)$$

where

$$K^A(x_{Bj},Q^2,y_A,z_1^{(A)}) = \frac{4\alpha_{\mathrm{em}}^2}{Q^4}\frac{\pi}{x_{Bj}}\cdot\left(\frac{y}{y_A}\right)^2\left[\frac{y_A^2}{2}+(1-y_A)-\frac{k_1^2 x_{Bj}^2 y_A^2}{z_1^{(A)2}Q^2}\right] \qquad (2)$$

with

$$y_A = \frac{k_1\cdot q}{k_1\cdot k_e}\ , \quad x_A = \frac{x_{Bj}}{z_1^{(A)}}, \quad z_1^{(A)} = \frac{k_1\cdot q}{m_N\nu}\ . \qquad (3)$$

Here k_1 is the four-momentum of the bound nucleon, $q^2 = (E_e - E_{e'})^2 - (\mathbf{k}_e - \mathbf{k}_{e'})^2 = -Q^2$ and, finally, $n_0^{A,\mathrm{FSI}}(\mathbf{P}_{A-1})$ is the distorted momentum distribution of the bound nucleon

$$n_0^{A,\mathrm{FSI}}(\mathbf{P}_{A-1}) = \frac{1}{2J_A+1}$$

$$\sum_{\mathcal{M}_A,\mathcal{M}_{A-1}}\left|\int \mathrm{d}\mathbf{r}'_1 \mathrm{e}^{\mathrm{i}\mathbf{P}_{A-1}\mathbf{r}'_1}\langle\Psi^0_{J_{A-1},\mathcal{M}_{A-1}}(\{\mathbf{r}'_i\})|S_{\mathrm{FSI}}^{XN}|\Psi^0_{J_A,\mathcal{M}_A}(\mathbf{r}'_1,\{\mathbf{r}'_i\})\rangle\right|^2. \qquad (4)$$

In Eq. (4), the primed quantities denote intrinsic coordinates and the quantity $S_{\rm FSI}^{XN}$ is the debris-nucleon eikonal scattering S-matrix

$$S_{\rm FSI}^{XN} \equiv S_{\rm FSI}^{XN}(\mathbf{r}_1,\ldots,\mathbf{r}_A) = \prod_{i=2}^{A}\left[1-\theta(z_i-z_1)\Gamma(\mathbf{b}_1-\mathbf{b}_i,z_1-z_i)\right] \tag{5}$$

where the Q^2- and x_{Bj}-dependent profile function is

$$\Gamma^{XN}(\mathbf{b}_{1i},z_{1i}) \,=\, \frac{\sigma_{\rm eff}(z_{1i},Q^2,x_{Bj})}{4\,\pi\,b_0^2}\,\exp\left[-\frac{\mathbf{b}_{1i}^2}{2\,b_0^2}\right], \tag{6}$$

with $\mathbf{r}_{1i} = \{\mathbf{b}_{1i},z_{1i}\}$ being $z_{1i} = z_1 - z_i$ and $\mathbf{b}_{1i} = \mathbf{b}_1 - \mathbf{b}_i$. It can be seen that, unlike the standard Glauber eikonal approach [15], the profile function Γ^{XN} depends not only on the transverse relative separation but also on the longitudinal separation $z_{1,i} = z_1 - z_i$ due to the z- (or time) dependence of the effective cross section $\sigma_{\rm eff}(z_{1i},Q^2,x_{Bj}) \equiv \sigma_{\rm eff}(z_{1i})$. The cross section (1) describes the process in which, after the hard interaction of γ^* with a quark of the so called "active" nucleon "N", a nucleon debris is created, composed by a nucleon N_1 arising from target fragmentation, and a color string which propagates and hadronizes giving rise to an increasing with time (distance) number of pions. The interaction of the hadronizing debris with the nucleons of $(A-1)$ is described by an effective cross section $\sigma_{\rm eff}(z)$, which depends on the total energy of the debris, $W_X^2 \equiv P_X^2$; if the energy is not high enough, the hadronization procedure can terminate inside the nucleus $(A-1)$, after which the number of produced hadrons and the cross section $\sigma_{\rm eff}(z)$ remain constant. The effective debris-nucleon cross section derived in [8] has the following form

$$\sigma_{\rm eff}(z) \,=\, \sigma_{\rm tot}^{NN} \,+\, \sigma_{\rm tot}^{\pi N}\left[\,n_M(z) \,+\, n_G(z)\,\right] \tag{7}$$

where the Q^2- and x_{Bj}-dependent quantities $n_M(z)$ and $n_G(z)$ are the pion multiplicities due to the breaking of the color string and to gluon radiation, respectively, whose explicit forms are given in Ref. [8].

2. *Comparison between experimental data and theoretical calculations for the process* $^2\mathrm{H}(e,e'p)X$

Experimental data on the process $^2\mathrm{H}(e,e'p)X$ have recently been obtained at Jlab [9, 10] in the following kinematical regions: beam energy $E_e = 5.75$ GeV, four-momentum transfer 1.2 $(\mathrm{GeV}/c)^2 \lesssim Q^2 \lesssim 5.0$ $(\mathrm{GeV}/c)^2$, recoiling proton momentum 0.28 GeV/$c \lesssim |\mathbf{p}_p| \leq 0.7$ GeV/c, proton emission angle $-0.8 \leq \cos\theta_{\mathbf{p}} \leq 0.7$ ($\theta_{\widehat{\mathbf{p}_p\cdot\mathbf{q}}} \equiv \theta_{\mathbf{p}}$), invariant mass of the produced hadronic state 1.1 GeV $\leq W_X \leq$ 2.7 GeV, with $W_X^2 = (k_1+q)^2 = (P_D - p_p + q)^2$ (in what follows, all deuteron quantities: cross sections, mass, momentum, etc. will be denoted by the case D).

The experimental data have been plotted in terms of the reduced cross section

$$\sigma^{\rm red}(x_{Bj},Q^2,\mathbf{p}_p)=\frac{1}{K^A(x_{Bj},Q^2,y_A,z_1^{(A)})}\left(\frac{y}{y_D}\right)^2\frac{{\rm d}\sigma^{D,{\rm exp}}}{{\rm d}x_{Bj}{\rm d}Q^2{\rm d}\mathbf{p}_p} \tag{8}$$

which, considering Eq. (1) would be

$$\sigma^{\rm red}(x_{Bj},Q^2,\mathbf{p}_p)=\left(\frac{y}{y_D}\right)^2 z_1^{(D)}F_2^{N/D}(x_D,Q^2,k_1^2)\,n_0^{D,{\rm FSI}}(\mathbf{p}_p) \tag{9}$$

in agreement with the experimental definition of Ref. [9]. A comparison between theoretical calculations (performed using the AV18 potential [16]) and the experimental data plotted *vs* $\cos\theta_{\mathbf{p}}$ at fixed values of Q^2, W_X and $|\mathbf{p}_p|$, is presented in Fig. 3, which clearly shows that: i) apart from the very backward emission,

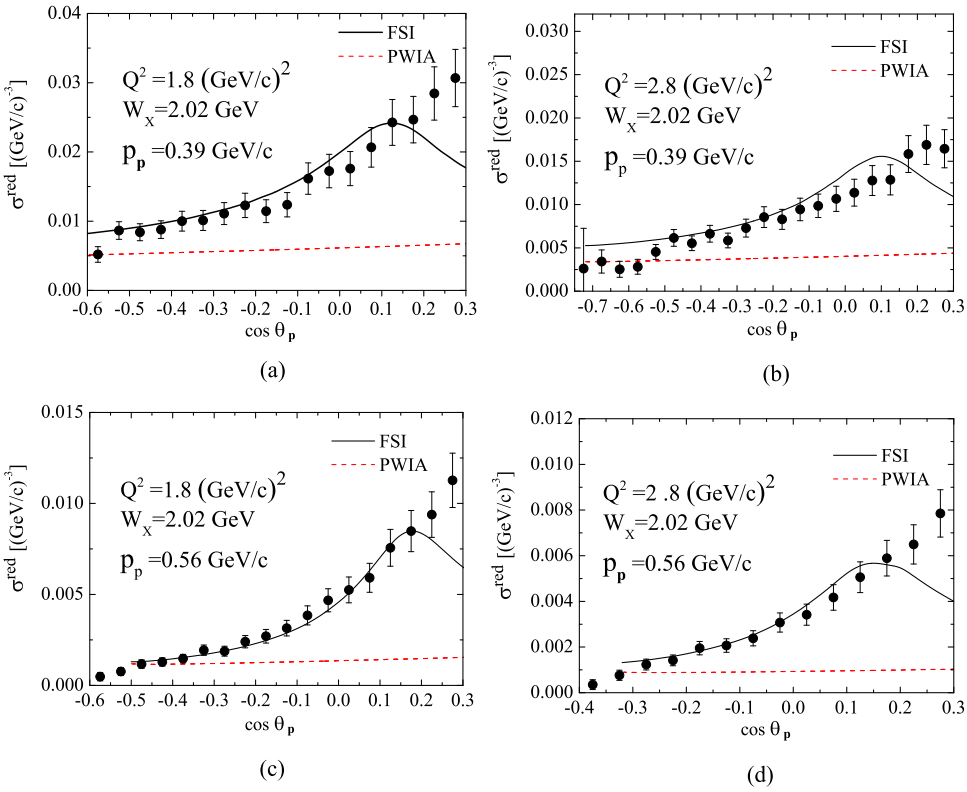

Fig. 3. The theoretical reduced cross section, Eq. (9), vs. cos$\theta_{\widehat{\mathbf{q}\cdot\mathbf{p}_p}}$ ($\theta_{\widehat{\mathbf{q}\cdot\mathbf{p}_p}}\equiv\theta_p$) compared with the experimental data of Refs. [9, 10]. Each figure shows the reduced cross section calculated at fixed values of the four momentum transfer Q^2, the invariant mass W_X of the hadronic state X, and the momentum $|\mathbf{p}_p|\equiv p_p$ of the detected proton. The error bars represent the sum in quadrature of statistical and systematic errors given in Refs. [9, 10] (after Ref. [12]).

the experimental data are dominated by the FSI; ii) the model of FSI of Refs. [8, 11, 12] provides a satisfactory description of the experimental data in the backward direction and also around $\theta_{\mathbf{p}} \simeq 90^\circ$ (a comparison of theoretical results and experimental data in the full range of kinematics of Refs. [9, 10] will be presented elsewhere; iii) in the forward direction ($\theta_{\mathbf{p}} \lesssim 80^\circ$) the spectator mechanism fails to reproduce the data and it is clear that other production mechanisms are playing a role in this region. For such a reason in what follows only the region ($\theta_{\mathbf{p}} \gtrsim 80^\circ$) will be considered, where useful information on both the hadronization mechanism and the EMC effect can in principle be obtained, provided the data are analyzed in the proper way, i.e. getting rid of EMC effects, in the former case, and of nuclear effects, in the latter case.

3. *The process $A(e, e'\,(A-1))X$ on few body systems and complex nuclei*

We have considered the processes ^{3}He$(e, e'd)X$ and ^{40}Ca$(e, e'\ ^{39}$K$)X$. Calculations have been performed using for ^{2}H and ^{3}He [17] wave functions corresponding to a realistic interaction [16], whereas for heavier nuclei single particle mean field wave functions have been adopted. The form of the nucleon structure function $F_2^{N/A}$ is from Ref. [18], with the nucleon off-mass shell within the x-rescaling model, i.e. $x_A = x_{Bj}/z_1^{(A)}$ where $z_1^{(A)} = k_1 \cdot q/(m_N \nu)$, with $k_1^0 = M_A - \sqrt{(M^*_{A-1})^2 + \mathbf{P}_{A-1}{}^2}$. In Fig. 4, the ^{3}He and ^{40}Ca distorted momentum distributions given by Eq. (4) are shown at parallel ($\theta_{\widehat{\mathbf{P}_{A-1}\cdot\mathbf{q}}} \equiv \theta = 180^0$) and perpendicular ($\theta_{\widehat{\mathbf{P}_{A-1}\cdot\mathbf{q}}} \equiv \theta = 90^0$) kinematics. The sensitivity of the distorted momentum distributions upon different models of the debris-nucleon cross section is illustrated in Fig. 5.

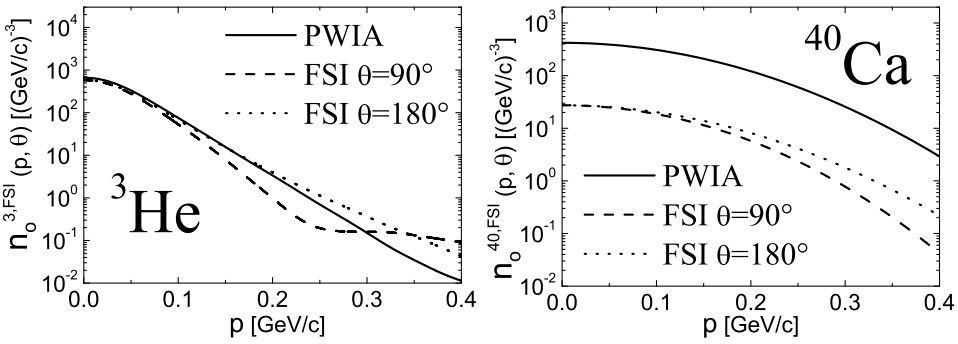

Fig. 4. The distorted momentum distributions $n_0^{A,\mathrm{FSI}}(\mathbf{P}_{A-1})$ (Eq. (4)) for ^{3}He and ^{40}Ca. The full curves correspond to the PWIA ($\sigma_{\mathrm{eff}} = 0$) and the dotted and dashed curves to the FSI ($\sigma_{\mathrm{eff}} \neq 0$) in parallel ($\theta_{\widehat{\mathbf{q}\mathbf{p}_p}} \equiv \theta = 180^0$) and perpendicular ($\theta_{\widehat{\mathbf{q}\mathbf{p}_p}} \equiv \theta = 90^0$) kinematics, respectively. Here $|\mathbf{P}_{A-1}| \equiv p$.

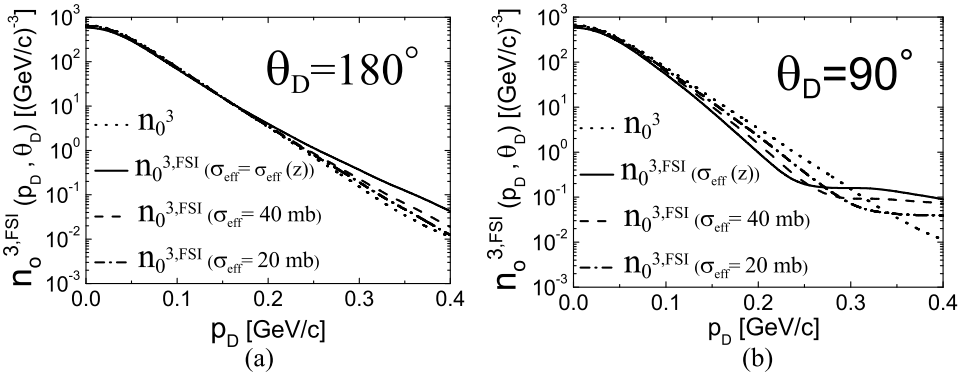

Fig. 5. The distorted momentum distributions $n_0^{3,\mathrm{FSI}}(\mathbf{P}_{A-1})$ *(Eq. (4) with* $\mathbf{P}_{A-1} \equiv \mathbf{p}_D$*) in the process* $^3\mathrm{He}(e,e'D)X$ *in parallel (*$\theta_{\widehat{\boldsymbol{P}_{A-1}\cdot\boldsymbol{q}}} \equiv \theta_D = 180^0$*) (a) and perpendicular (*$\theta_{\widehat{\boldsymbol{P}_{A-1}\cdot\boldsymbol{q}}} \equiv \theta_D = 90^0$*) (b) kinematics calculated with different effective debris-nucleon cross sections in Eq. (6): the effective debris-nucleon cross section* $\sigma_{\mathrm{eff}}(z) \equiv \sigma_{\mathrm{eff}}(z, Q^2, x_{Bj})$ *(full line) and two constant cross sections (dashed and dot-dashed lines). The undistorted momentum distribution* $n_0^3(|\mathbf{P}_{A-1}|)$ *is shown by the dotted line. Calculations have been performed at the following kinematics:* $E_e = 12$ GeV, $Q^2 = 6$ GeV$^2/c^2$ *and* $W_X^2 = 5.8$ GeV^2 *(after Ref. [12]).*

It can be seen that, in the case of few-nucleon systems, FSI is particularly relevant at high momentum values, whereas for complex nuclei the momentum distributions are strongly affected also at low momentum, with a resulting strong decrease of the survival probability of $(A-1)$ (see Ref. [8] for more details). In order to obtain information on hadronization mechanisms minimizing, at the same time, possible contaminations from the poor knowledge of the neutron structure function, the ratio of the cross sections for two different nuclei A and A', measured at the same value of x_{Bj}, should be considered [7, 12], *viz*

$$\frac{\sigma^{A,\mathrm{exp}}(x_{Bj}, Q^2, |\mathbf{P}_{A-1}|, z_1^{(A)}, y_A)}{\sigma^{A',\mathrm{exp}}(x_{Bj}, Q^2, |\mathbf{P}_{A-1}|, z_1^{(A')}, y_{A'})} \to \frac{n_0^{(A,\mathrm{FSI})}(\mathbf{P}_{A-1})}{n_0^{(A',\mathrm{FSI})}(\mathbf{P}_{A-1})} \equiv R(A, A', \mathbf{P}_{A-1}) \quad (10)$$

where the last step is strictly valid only in the Bjorken limit. However, as discussed in detail in Refs. [7, 12], the ratio (10) is governed by the ratio of the distorted momentum distributions, and any reasonably expected A-dependence of $F_2^{N/A}(x_A, Q^2, k_1^2)$, through x_A, will not affect it. The ratio (10) for $A = 2$, $A' = 3$ and $A' = 40$ is shown in Fig. 6. Since the low-momentum part of the momentum distributions is very well known, the experimental observation of strong deviations from the PWIA predictions (full curves) would provide information on the debris-nucleon interaction and, consequently, on hadronization. Experiments on heavier nuclei, particularly at perpendicular kinematics and $|\mathbf{P}_{A-1}| \simeq 0.2 \div 0.3$ GeV/c (*cf.* Fig. 6, where the effects of FSI are expected to be more relevant [8], would be extremely useful to clarify the hadronization mechanisms.

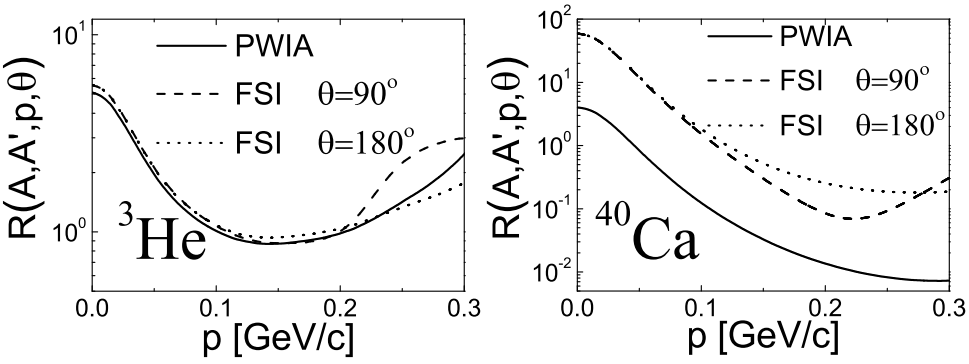

Fig. 6. The ratio (10) with $A = 2$, $A' = 3$ (left) and $A = 2$, $A' = 40$ (right). Full curve*: PWIA ($\sigma_{\rm eff} = 0$);* dashed and dotted curves*: FSI ($\sigma_{\rm eff} \neq 0$) in perpendicular and parallel kinematics, respectively ($p \equiv |\boldsymbol{p}| \equiv |\boldsymbol{P}_{A-1}|$).*

In order to tag the EMC effect, i.e. if, how, and to what extent the nucleon structure function in the medium differs from the free structure function, one has to get rid of the distorted nucleon momentum distributions and other nuclear structure effects by considering a quantity which would depend only upon $F_2^{N/A}(x_A, Q^2, k_1^2)$. This can be achieved by introducing the ratio of the cross sections on the nucleus A measured at two different values of the Bjorken scaling variables x_{Bj} and x'_{Bj}, leaving unchanged all other quantities in the two cross sections, i.e. the ratio

$$\begin{aligned} & \frac{\sigma^{A,\exp}(x_{Bj}, Q^2, |\mathbf{P}_{A-1}|, z_1^{(A)}, y_A)}{\sigma^{A,\exp}(x'_{Bj}, Q^2, |\mathbf{P}_{A-1}|, z_1^{(A)}, y_A)} \\ \rightarrow \quad & \frac{F_2^{N/A}(x_A, Q^2, k_1^2)}{F_2^{N/A}(x'_A, Q^2, k_1^2)} \equiv R(x_{Bj}, x'_{Bj}, |\mathbf{P}_{A-1}|). \end{aligned} \tag{11}$$

The quantity (11) for the processes $^3\mathrm{He}(e, e'D)X$ and $^{40}\mathrm{Ca}(e, e'\,^{39}\mathrm{K})X$ were calculated in the following kinematical range: $2\ \mathrm{GeV}^2 \lesssim W_X^2 \lesssim 10\ \mathrm{GeV}^2$ and $Q^2 = 8\,(\mathrm{GeV}/c)^2$. At each value of W_X, we have changed $|\mathbf{P}_{A-1}|$ from zero to $|\mathbf{P}_{A-1}| = 0.5\ \mathrm{GeV}/c$, obtaining for different values of $|\mathbf{P}_{A-1}|$ different values of x_{Bj}. In order to minimize the effects of FSI, the angle $\theta_{\widehat{\mathbf{P}_{A-1}\cdot\mathbf{q}}} \equiv \theta_{A-1}$ has been chosen in the backward direction, $\theta_{\widehat{\mathbf{P}_{A-1}\cdot\mathbf{q}}} \equiv \theta_{A-1} \sim 145^o$ (*cf.* Fig. 7). Within such a kinematics, the effective cross section $\sigma_{\rm eff}(z_{1i}, x_{Bj}, Q^2)$ is the same for different values of W_X and, correspondingly, the distorted momentum distributions $n_0^{A,\mathrm{FSI}}$ will depend only on $|\mathbf{P}_{A-1}|$ and cancel in the ratio (11). In this way, all nuclear structure effects, except possible effects of in-medium deformations of the nucleon structure function $F_2^{N/A}$, are eliminated, and one is left with a ratio which depends only on the nucleon structure function $F_2^{N/A}$. Calculations have been performed using three different structure functions $F_2^{N/A}(x_A, Q^2, k_1^2)$, namely:

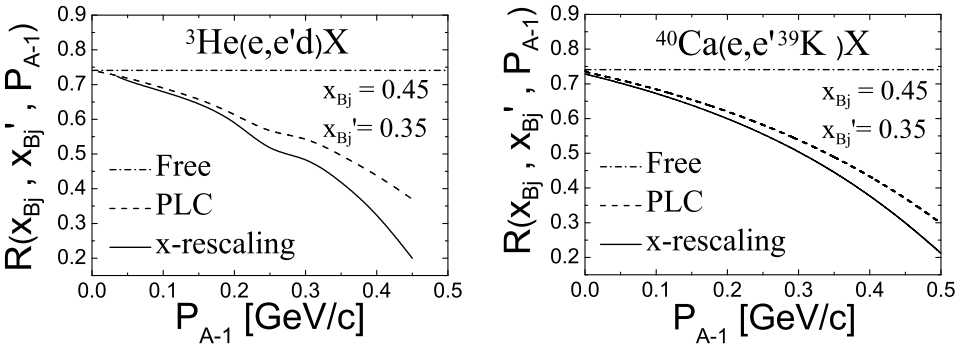

Fig. 7. The ratio (11) corresponding to the process $^3\mathrm{He}(e,e'd)X$ *and to the process* $^{40}\mathrm{Ca}(e,e'\,^{39}K)X$ *calculated at two values of the Bjorken scaling variable* x_{Bj} *and with different nucleon structure functions: i) Free structure function (dot-dashed line):* $F_2^{N/A}\left(x^A\right) = F_2^{N/A}\left(x_{Bj}\right)$*; ii) off mass-shell (x-rescaling) structure function (full line):* $F_2^{N/A}\left(x^A\right) = F_2^{N/A}\left(x_{Bj}/z_1^A\right)$ *with* $z_1^A = k_1 \cdot q/(m_N\,\nu)$ *and* $k_1^0 = M_A - \sqrt{\left(M^*_{A-1}\right)^2 + \mathbf{P}^2_{A-1}}$*; iii) structure function with reduction of point-like configurations (PLC) in the medium depending on the nucleon virtuality* $v(\mathbf{k}_1, E)$ *(Eq. (13)) [19] (dashed line):* $F_2^{N/A}\left(x^A\right) = F_2^{N}\left(x_{Bj}/z_1^N\right) \cdot \delta_A(x_{Bj}, v(\mathbf{k}_1, E))$ *with* $z_1^A = k_1 \cdot q/(m_N\,\nu)$ *and* $k_1^0 = M_A - \sqrt{m_N^2 + \mathbf{P}^2_{A-1}}$.

1) the free nucleon structure function from Ref. [18], exhibiting no EMC effects;

2) the nucleon structure function pertaining to the x-rescaling model with the nucleon off-mass shell, i.e. $F_2^{N/A}(x_A, Q^2, k_1^2) \to F_2^N(x_A, Q^2) = F_2^N(\frac{x_{Bj}}{z_1^A}, Q^2)$, where $z_1^A = k_1 \cdot q/(m_p\nu)$ with $k_1^0 = M_A - \sqrt{{M^*_{A-1}}^2 + {\mathbf{k}_1}^2}$;

3) the structure function from Ref. [19], which assumes that the reduction of nucleon point like configurations (PLC) in medium (see Ref.[20]) depends on the nucleon virtuality

$$F_2^{N/A}(x_A, Q^2, k_1^2) \to F_2^{N/A}\left(x_{Bj}/z_1^N, Q^2\right)\delta_A(x_{Bj}, v(|\mathbf{k_1}|, E)), \qquad (12)$$

where $z_1^N = (m_N + |\mathbf{P}_{A-1}|\cos\theta_{A-1})/m_N$. Here the reduction of PLC is given by the quantity $\delta_A(x_{Bj}, v(\mathbf{k}, E))$, which depends on the nucleon virtuality (see [19]),

$$v(|\mathbf{k}_1|, E) = \left(M_A - \sqrt{(M_A - m_N + E)^2 + \mathbf{k}_1^2}\right)^2 - \mathbf{k}_1^2 - m_N^2. \qquad (13)$$

where E is the nucleon removal energy. It should be stressed that the two medium-dependent structure functions provide similar results for the inclusive cross section and that our aim is to answer the question as to whether the SIDIS experiment we are proposing could discriminate between the two models. The results of calculations corresponding to the kinematics $E_e = 12$ GeV, $Q^2 = 8$ (GeV/c)^2, $\theta_{A-1} = 145^o$, $x_{Bj} = 0.45$, $x'_{Bj} = 0.35$, are presented in Fig. 7. It can be seen that the discrimination between different models of the virtuality dependence of $F_2^{N/A}(x_A, Q^2, k_1^2)$ can indeed be achieved by a measurement of the ratio (11); as a matter of fact at $|\mathbf{P}_{A-1}| \simeq 0.4$ GeV/c, the two structure functions differ by about 40 %.

4. Summary and conclusions

We have considered the SIDIS process $A(e, e'(A-1))X$ on complex nuclei proposed in Ref. [7] within the spectator model and the PWIA, and extended in Ref. [8] by the inclusion of the FSI between the hadronizing debris and the nucleons of the detected nucleus $(A-1)$. The results of our calculations for the process ^{2}H$(e, e'p)X$ show that the experimental data can be well reproduced in the kinematics when the proton is emitted mainly backward in the range $70^0 \lesssim \theta_{\mathbf{p}} \lesssim 145^0$, with the effects of FSI being very small in the very backward direction, and dominating the cross section around $\theta_{\mathbf{p}} \simeq 90^0$. It is very gratifying to see that the experimental data can be reproduced in a wide kinematical region, which makes us confident of the correctness of the spectator model and the treatment of the FSI between the nucleon debris and the detected proton. At emission angles $\theta_{\mathbf{p}} \lesssim 70^0$, the number of detected proton is much higher than our predictions, which is clear evidence of the presence of production mechanisms different from the spectator one. Among possible mechanisms leading to forward proton production, target and/or current fragmentation should be the first process to be taken into account. The first one has been analyzed in Ref. [14], finding that it contributes only at forward angles and at proton momentum values much higher than the ones typical of the Jlab kinematics. The contribution from current fragmentation effects is under investigation. The process on nuclei with $A > 2$ would be extremely interesting, since the only mechanism for producing a recoiling $(A-1)$ nucleus would be the spectator mechanism. These experiments, as stressed in Ref. [8], would be very helpful to clarify the mechanism of the early stage of hadronization at short formation times without being affected by cascading processes, unlike the DIS inclusive hadron production $A(e, e'h)X$ where most hadrons with small momentum originate from cascading of more energetic particles. We have illustrated, by measuring the reduced cross section on two different nuclei at the same value of the detected momentum, how the validity of the spectator mechanism and information on the survival probabilities of the spectator nuclei, i.e. on the hadronization mechanism, could be obtained; moreover, by measuring the cross section on the same nucleus, but at two different values of x_{Bj}, the EMC effect could be tagged. Experimental investigation of the processes ^{2}H$(e, e'p)X$, ^{3}He$(e, e'\,d)X$, ^{4}He$(e, e'\,^3$H$)X$ and ^{4}He$(e, e'\,^3$He$)X$ would be

extremely interesting and useful, and it is gratifying to see that they are planned to be performed thanks to the developments of proper recoil detectors [13].

Acknowledgements

We would like to thank Sebastian Kuhn for providing the experimental data that we used to produce Fig. 3 and for many useful discussions and suggestions. Discussions with Alberto Accardi, Kawtar Afidi, Boris Kopeliovich and Veronica Palli are also gratefully acknowledged. Calculations have been performed at CASPUR facilities under the Standard HPC 2010 grant *SRCnuc*. One of us (L.P.K) thanks the Italian Ministry of Education, University and Research (MIUR), and the Department of Physics, University of Perugia, for support through the program "Rientro dei Cervelli".

References

[1] P. R. Norton, Rep. Prog. Phys. **66** (2003) 1253.

[2] A. Accardi, F. Arleo, W. K. Brooks, D. D'Enterria and V. Muccifora, Riv. Nuovo Cimento Soc. Ital. Fis. **032** (2010) 439.

[3] B. Z. Kopeliovich, J. Nemchik, E. Predazzi and A. Hayashigaki, Eur. Phys. J. A **19**, S1 (2004) 111.

[4] E. Wang and X.-N. Wang, Phys. Rev. Lett. **89** (2002) 162301.

[5] A. Accardi, V. Muccifora and H.J. Pirner, Nucl. Phys. A **720** (2003) 131.

[6] T. Falter, W. Cassing, K. Gallmeister and U. Mosel, nucl-th/0303011; nucl-th/0406023.

[7] C. Ciofi degli Atti, L. P. Kaptari and S. Scopetta, Eur. Phys. J. A **5** (1999) 191.

[8] C. Ciofi degli Atti and B. Kopeliovich, Eur. Phys. J. A **17** (2003) 133.

[9] A. V. Klimenko, S. E. Kuhn, C. Butuceanu, K. S. Egiyan et al., Phys. Rev. C **73** (2006) 035212.

[10] S. E. Kuhn, private communication.

[11] C. Ciofi degli Atti, L. P. Kaptari and B. Z. Kopeliovich, Eur. Phys. J. A **19** (2004) 145.

[12] C. Ciofi degli Atti and L. P. Kaptari, arXiv: nucl-th 1011-5960v2, to appear in Phys. Rev.

[13] See e.g. *Nuclear Exclusive and Semi-inclusive Physics with a New CLAS12 Low Energy Recoil Detector*, LOI to the PAC Jlab, K. Hafidi et al., Spokespersons and private communication.

[14] V. Palli, C. Ciofi degli Atti, L. P. Kaptari, C. B. Mezzetti and M. Alvioli, Phys. Rev. C **80** (2009) 054610.

[15] R. J. Glauber, in *Lectures in Theoretical Physics*, edited by W. E. Brittin et al., vol. 1, Interscience Publishers, New York (1959) p. 315.

[16] R. B. Wiringa, V. G. J. Stoks and R. Schiavilla, Phys. Rev. C **51** (1995) 38.

[17] A. Kievsky, S. Rosati and M. Viviani, Phys. Rev. Lett. **82** (1999) 3759;
A. Kievsky, private communication.

[18] B. Adeva et al. (SM Collaboration), Phys. Lett. B **412** (1997) 414.

[19] C. Ciofi degli Atti, L. P. Kaptari, L. L. Frankfurt and M. I. Strikman, Phys. Rev. C **76** (2007) 055206.

[20] L. L. Frankfurt and M. I. Strikman, Phys. Rep. **160** (1988) 235.

OZNAČAVANJE EMC UČINAKA I MEHANIZAMA HADRONIZACIJE POLUINKLUZIVNIM DUBOKO-NEELASTIČNIM RASPRŠENJEM NA JEZGRAMA

Poluinkluzivno duboko-neelastično raspršenje elektrona na jezgri A uz detekciju spore jezgre $(A-1)$ u osnovnom ili nisko-uzbudnom stanju, tj. proces $A(e,e'(A-1))X$, pruža vrijedne podatke o nastanku EMC učinka i mehanizama hadronizacije. Daje se teorijski opis procesa i predstavljaju ishodi više računa za malonukleoske sustave i za veće jezgre.